Materials and Structures (2014) 47:1373–1390
DOI 10.1617/s11527-014-0362-z

ORIGINAL ARTICLE

Digital image correlation techniques to investigate strain fields and cracking phenomena in asphalt materials

William G. Buttlar · Brian C. Hill · Y. Richard Kim · M. Emin Kutay · Anne Millien · Antonio Montepara · Glaucio H. Paulino · Christophe Petit · Ion Octavian Pop · Elena Romeo · Riccardo Roncella · Seyed Amirshayan Safavizadeh · Gabriele Tebaldi · Andrew Wargo

Received: 14 November 2013 / Accepted: 12 June 2014 / Published online: 9 July 2014

Abstract This paper is the outcome of a specific task group of the RILEM Technical Committee 241-MCD "Mechanisms of Cracking and Debonding in Asphalt and Composite Pavements". The group on "Advanced Measurement Techniques" was established in 2011 to investigate DIC applications for non-destructive and non-contact measurements of strain fields during laboratory testing. The paper illustrates different DIC/optical flow applications in measuring strain distribution during laboratory testing. Specific applications of DIC for evaluating crack initiation and crack propagation in asphalt materials are presented.

Keywords Asphalt mixture · Digital image correlation · Optical flow · Mode I fracture · Mode II fracture · Debonding

W. G. Buttlar · B. C. Hill · G. H. Paulino
University of Illinois at Urbana-Champaign, Urbana, IL, USA

Y. R. Kim · S. A. Safavizadeh · A. Wargo
North Carolina State University, Raleigh, NC, USA

M. E. Kutay
Michigan State University, East Lansing, MI, USA

A. Millien · C. Petit · I. O. Pop
University of Limoges, Limoges, France

A. Montepara · E. Romeo (✉) · R. Roncella · G. Tebaldi
University of Parma, Parma, Italy
e-mail: elena.romeo@unipr.it

1 Introduction

In the last decade full-field non-contact optical measurement techniques have become increasingly popular to investigate fracture phenomena in asphalt materials [21]. Kim and Wen [13] first proposed the use of a DIC technique as a possible displacement/strain measurement method for asphalt mixtures. They applied the DIC technique to determine the proper gauge length for a 100-mm diameter IDT specimen. They highlighted that if the gauge length is too long for surface-mounted LVDTs, the stress concentration under the loading strips can cause errors in the strain calculation. Masad et al. [16–18] and Tashman et al. [29] used both digital imaging and X-ray computed tomography techniques to evaluate the microstructure of HMA in terms of aggregate orientation and air voids concentration, as well as strain distribution. They found that the percent of air voids is the main factor that controls strain distribution. Seo et al. [24] adopted the DIC technique to measure local and global deformations in the fracture process zone (FPZ) using a double-notched constant crosshead rate direct tension test. They investigated the effect of the notch size on process zone evolution using three different types of notches. Hartman and Gilchrist [10] used the DIC technique to measure the physical crack length developing during four point bending fatigue test on asphalt specimens. Chehab et al. [5] calibrated the viscoelastoplastic continuum damage (VEPCD) model, developed by Kim and Little [12] and Chehab

et al. [4] for the behavioral prediction of asphalt-aggregate mixtures subjected to tensile stresses using DIC. The imaging technique allowed to extend the validation of the VEPCD model, predicting strains accurately even beyond the localization of crack initiation up to the instance of macrocrack development and propagation, which was not possible using solely LVDT. Birgisson et al. [1, 3] used DIC to validate the theory at the base of the visco-elastic fracture mechanics-based crack growth law, entitled "HMA Fracture Mechanics" developed by Zhang et al. [32] and Roque et al. [22] which identifies a fundamental crack growth threshold as the key element in defining the cracking mechanism and fracture resistance of asphalt mixtures. Thiago and Kim [30] presented an integrated approach incorporating DIC test results at the local fracture process zone, with numerical cohesive zone fracture modeling to characterize fundamental fracture properties of asphalt mixtures subjected to a wide range of loading rates at intermediate temperature conditions. They concluded that the DIC technique can accurately capture the crack tip fracture process and can be simply incorporated with the numerical cohesive zone fracture modeling to identify local fracture characteristics of asphalt materials at intermediate service temperatures.

This paper summarizes the most significant experimental studies performed using DIC-based techniques on asphalt mixture fracture phenomena, in particular Mode I fracture, Mode II fracture and debonding.

2 Matching algorithm commonly applied to DIC strain evaluation

The basic principle of DIC is the tracking of the same points (or pixels) between two consecutive images (i.e. before and after loading.). The feature tracking is usually achieved using Area Based Matching (ABM), a technique for the extraction of image correspondences based on similarities between grey values. In ABM, each image point to be matched is the center of a small window of pixels (template) in an not-deformed reference image (master image), which usually corresponds to the first image in the sequence of frames. The grey values of the template are statistically compared with those of an equally sized window of pixels (patch) in a deformed search image (slave image), which corresponds to another image in the sequence of frames. Two different approaches are usually adopted for the evaluation of the similarities between patch and template's grey values: Cross-Correlation and Least Squares Matching (LSM). The cross-correlation function tracks the interested point by shifting pixel by pixel the template window within a specific range in the patch window using a simple translation, while the Least Square Matching (LSM) method is based on the minimization of the squared differences of the grey values between patch and template (Differential method). More details are discussed by Romeo [21].

2.1 Specimen preparation and experimental setup

The specimen surface must show a random grey intensity distribution (i.e. random speckle pattern) to ensure a successful imaging acquisition and the subsequent application of the DIC method. Since asphalt mixtures do not exhibit a well-contrasted natural texture, the speckle pattern is usually artificially made applying thin white paint overprinted by a speckle pattern of black, resulting in a homogeneous randomly oriented texture. Care must be taken in ensuring thin enough layer thickness to avoid tracking the deformation of the paint film rather than the specimen deformation. The most suitable paint is a water-based one, which is lightly absorbed by the asphalt mixture, not affecting the real material behavior. The accuracy of displacement measurements is closely related to the quality of the speckle pattern on the specimen surface, which may demonstrate distinctly different grayscale distribution characteristics, such as different image contrasts or speckle sizes [14]. Images are acquired with a digital camera, directly connected with a personal computer, located on a support (possibly inside the climatic chamber of a material testing system), and placed with its optical axis normal to the specimen surface, imaging the planar specimen surface during loading. An adequate lighting system must provide adequate illumination of the specimen, especially if the camera is located inside the climatic chamber.

2.2 Accuracy and limitations

Previous work presented by Birgisson et al. [2] has shown that, with proper test set-up, accuracies up to

Table 1 Theoretical image system accuracy

ROI	1 cm	3 cm	5 cm	10 cm
Displ accuracy (μm)	0.08	0.23	0.38	0.77
ε grid 1 mm	0.011 %	0.033 %	0.054 %	0.109 %
ε grid 2 mm	0.005 %	0.016 %	0.027 %	0.054 %
ε grid 5 mm	–	0.007 %	0.011 %	0.022 %

1/100 of pixel can be achieved in terms of displacement evaluation. The theoretical εxx accuracy for locally homogeneous strain fields according to the Region of Interest (ROI) dimension and the mesh step size are listed in Table 1 assuming a sensor with 1300 × 1000 pixels and $\sigma u = 1/100$ pixel.

Since the recorded images are the 2D projection of the specimen surface, care must be taken in meeting appropriate requirements, otherwise the estimated motion of each image point multiplied by the magnification of the imaging system (in units of mm/pixel) will not accurately equal that of the actual physical point on the specimen surface. First of all, the specimen surface must be flat and remain in the same plane parallel to the CCD sensor target during loading [23, 26]. The out-of-plane motion of the specimen leads to a change in magnification of the recorded images, which, if not corrected appropriately, further yields additional in-plane displacements [2, 28]. Moreover, the imaging system should not suffer from geometric distortion, which can be removed using appropriate correction techniques [2, 27].

3 DIC application to mode I fracture in asphalt concrete

This section explores the application of DIC to study and to characterize mode I fracture behavior of asphalt concrete. Previous literature, such as Im et al. [11], applied DIC in mode I cases in asphalt materials without the combination of notched disk-shaped compact tension (DC(T)) specimens, consideration of the effects of temperature on strain localization, or the effects of modified asphalt binders. These variables significantly affect the material response to mechanical loads and DIC provides additional insight into their effects on the phenomenon of asphalt concrete fracture. This section will provide an analysis of two asphalt concrete mixtures tested in the asphalt concrete version of the DC(T) configuration at two testing temperatures using traditional global response measurements such as fracture energy and DIC strain fields.

3.1 Materials and methods

Two asphalt concrete mixtures, polymer modified and unmodified, were evaluated. The polymer modified asphalt mixture is a strain tolerant reflective cracking relief interlayer (RCRI) mixture with a nominal maximum aggregate size (NMAS) of 9.5 mm. Similarly, the unmodified asphalt mixture is a 9.5 mm NMAS with a PG 64-22 asphalt binder grade. Further details regarding these mixtures can be found in Dave et al. [8]. It should be noted that the materials tested in the current study were tested after approximately 5 years of storage in an enclosed building in metal containers. The materials were used in an accelerated pavement testing study, studying reflective cracking behavior and the effects of RCRI systems in mitigating reflective crack growth.

Fracture testing was completed using the aforementioned DC(T) configuration. This test configuration, according to Wagoner et al. [31], maximizes the fracture ligament area available in standard 150-mm diameter cylindrical asphalt field cores or laboratory specimens. Dave et al. [7] and Marasteanu and [15] demonstrated that data from the DC(T) test could be used to accurately predict asphalt mixture thermal cracking potential. The asphalt concrete geometry conforms to ASTM D7313-07. Testing was completed in accordance with the ASTM standard at a crack mouth opening displacement (CMOD) rate of 1 mm/min at temperatures of 0 and −12 °C. DC(T) CMOD fracture energy was calculated by evaluating the area under the load-CMOD curve and normalizing by the fractured surface area. Specimens were conditioned for 2 h at the testing temperature prior to test completion to ensure uniform specimen temperature and to avoid any condensation present on the surface imaged by DIC.

The DIC configuration consisted of a Tamron 50 mm lens, multiple LED light sources, and a Stingray F-201C CCD camera. The CCD camera is a 2 megapixel (MP) camera which captured images at a rate of 5 images/sec of size 1,624 pixels by 1,234 pixels. This camera was placed approximately 1 m from the sample in order to produce a region of interest

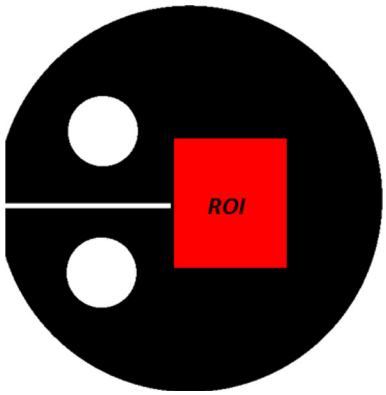

Fig. 1 DC(T) DIC qualitative depiction of ROI

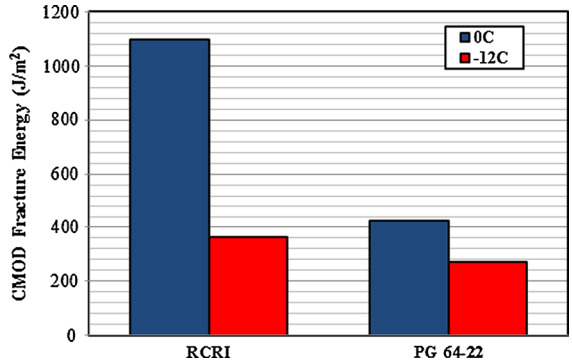

Fig. 2 DC(T) global results

(ROI) adequate with the phenomena investigated with the test. The ROI, shown in Fig. 1, was focused on a region centered just ahead of the notch tip to capture localized material straining. A distinct black and white speckle pattern was placed on the asphalt specimen surface prior to testing. Initially, specimen surfaces were painted black. Then, after approximately 60 min, a white speckle pattern was placed on the surface. Fracture testing was completed approximately 24 h after speckle pattern placement.

A full-field matching algorithm, previously employed by Shen and Paulino [25], was used in the current study prior to crack propagation. Further discussion of the calculation of displacement and strain fields can be found in that document.

3.2 Global analysis of results

The CMOD fracture energy results are provided in Fig. 2. As shown, the RCRI mixture possessed significantly higher fracture energy than the PG 64-22 mixture at 0 °C and slightly better (fracture energies differed by 89 J/m^2) at −12 °C. These results were anticipated as the RCRI mixture is formulated in a way which provides improved crack resistance through the use of a soft base binder and a very high level of polymer modification. However, due to the effects of aging, these results display a decrease in fracture energy as compared to the previous testing conducted by Dave et al. [8]. Although still under development, the following sections provide an initial demonstration of how the newly developed DIC tools can be used to gain additional insight into the fracture behavior of asphalt concrete as a function of temperature and binder type (unmodified vs. highly modified) when tested in the DC(T) configuration.

3.3 Analysis of DIC results

The DIC results in terms of strain fields in the vertical direction, ε_{yy}, are provided in Figs. 3, 4, 5, 6. Figure 3 presents the strain fields in the ROI immediately prior to crack propagation (3.25kN load). Figs. 4, 5, 6 show the strain fields present in the ROI at global loads of 3.0, 2.5, and 2.0kN, respectively. In both mixtures at both temperatures, the presence of the notch caused concentrated regions of strain to develop ahead of the notch tip, and the presence of loads being applied at the loading holes caused straining in the left, upper and lower portions of the ROI. The latter developed as a consequence of the loading pins deforming material around the loading holes, and the former due to the coalescence or localization of strains ahead of the notch tip prior to reaching the peak load capacity of the material. This strain path hypothesis can be seen in transitioning from the 2.0kN strain fields to the 3.0kN strain fields which show regions of straining at the upper and lower left corners which dissipate, likely due to material viscoelasticity, at these locations and flow toward the notch tip as the test progresses and load increases. Furthermore, asymmetry in the strain fields occurred due to the slight rotation in the specimen during testing. In the initial development of the DC(T) device, the size and location of the loading holes and the length of the notch were adjusted by trial-and-error to render the likelihood of failures at the loading holes as very minimal (a few percent of specimens experience this type of failure in the standard ASTM configuration). In future adaptations of the DC(T), such as in a current study to evaluate its

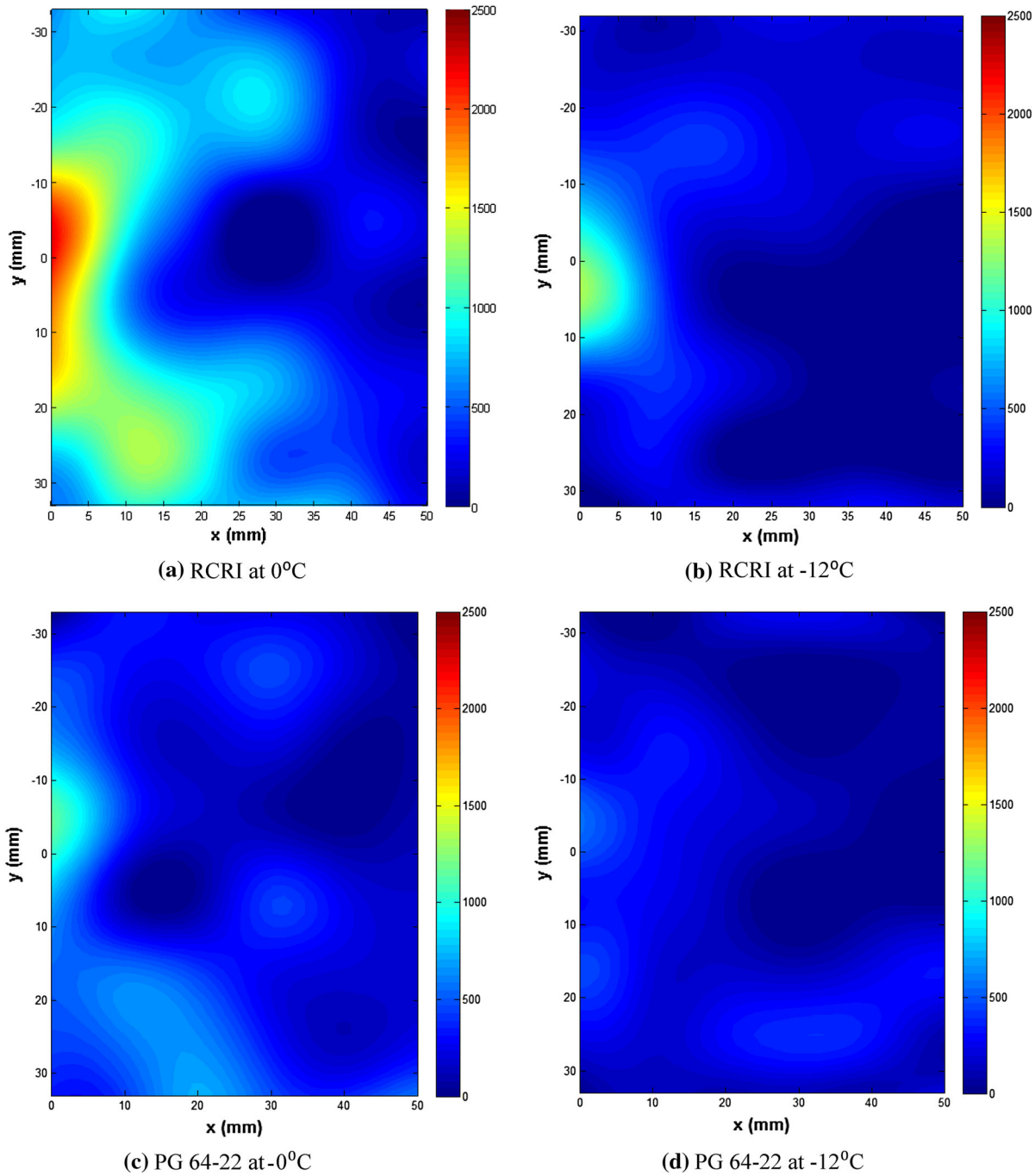

Fig. 3 DIC ε_{yy} fields immediately prior to crack propagation (με)—load range 2.0/3.0 kN

potential use in cyclic fracture testing, the DIC tool can be employed to optimize test geometry in a data-driven, efficient manner and reduce asymmetry in the strain field results.

From Fig. 3, the RCRI mixture at 0 °C produced the largest region of localized high strains (greater than 1,000με) amongst the two tested mixtures. This result was anticipated as this mixture should produce the greatest

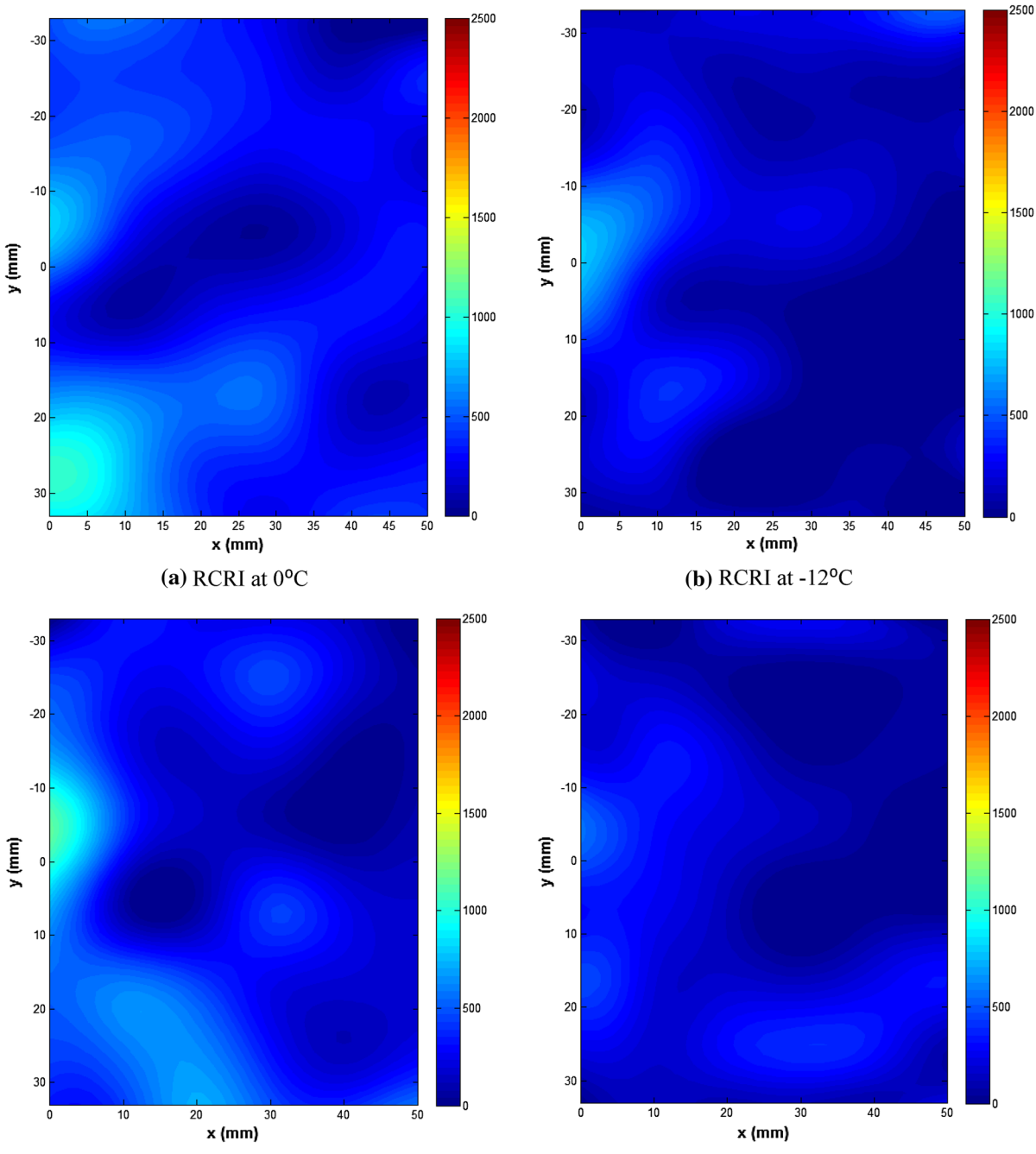

(a) RCRI at 0°C

(b) RCRI at -12°C

(c) PG 64-22 at -0°C

(d) PG 64-22 at -12°C

Fig. 4 DIC ε_{yy} Fields at 3.0 kN (με)

strain prior to crack propagation in comparison with the unmodified PG 64-22 asphalt mixture. These results differed from those present in Montepara et al. [19] which found that polymer modified asphalt mixtures produced smaller, distributed zones of strain in comparison with unmodified asphalt mixtures. The difference between that particular study and the current DIC application is likely due to the presence of the notch in the current study.

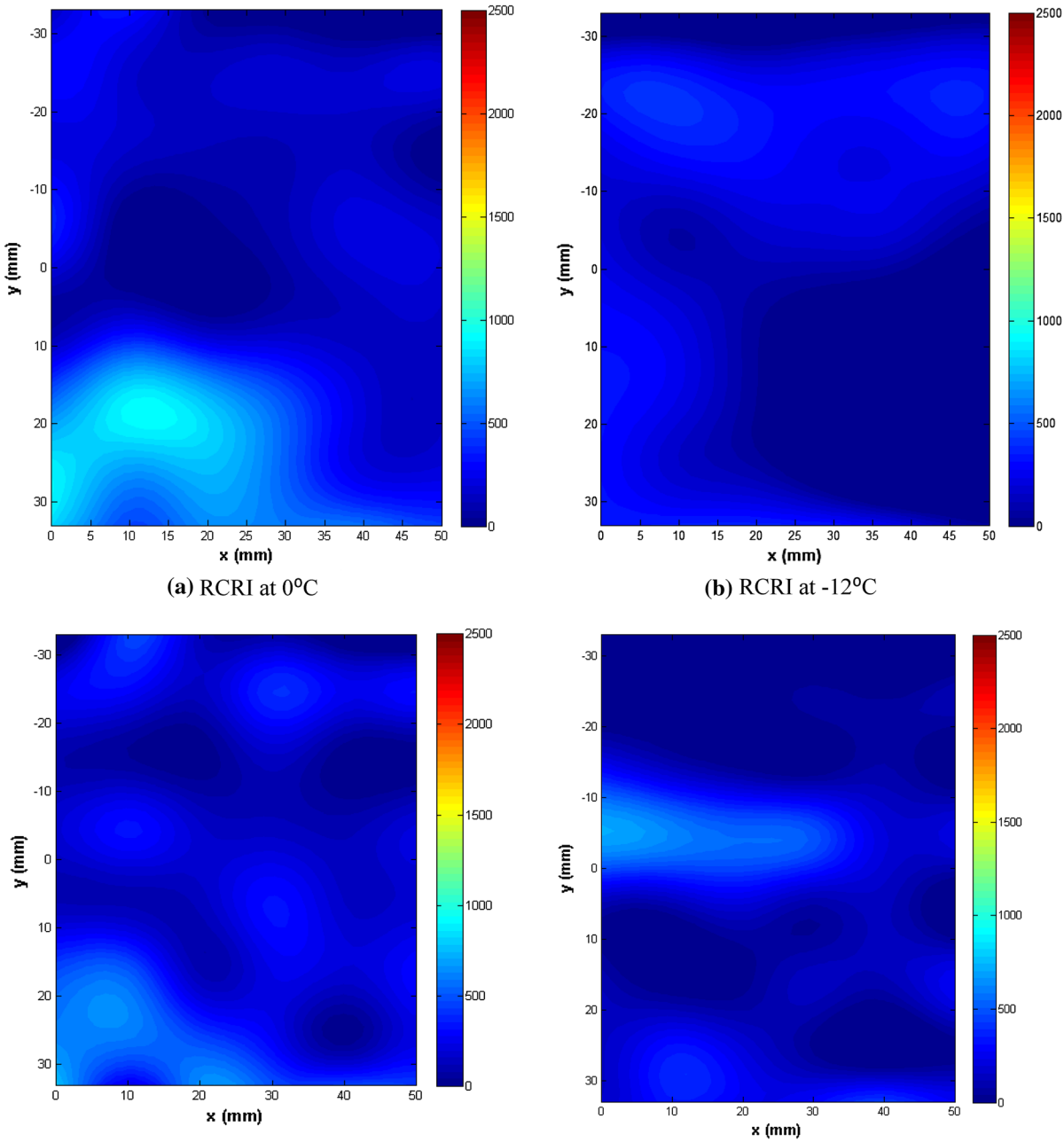

(a) RCRI at 0°C

(b) RCRI at -12°C

(c) PG 64-22 at -0°C

(d) PG 64-22 at -12°C

Fig. 5 DIC ε_{yy} Fields at 2.5 kN (με)

Temperature effects can also be seen in Fig. 3. Reduced temperatures led to reduced peak strains for a given load level and reduced strain localization zone lengths for both RCRI and PG 64-22 asphalt mixtures.

4 DIC application to mode II interface fracture in asphalt concrete

This section explores application of the DIC to study and to characterize mode II fracture behavior of asphalt

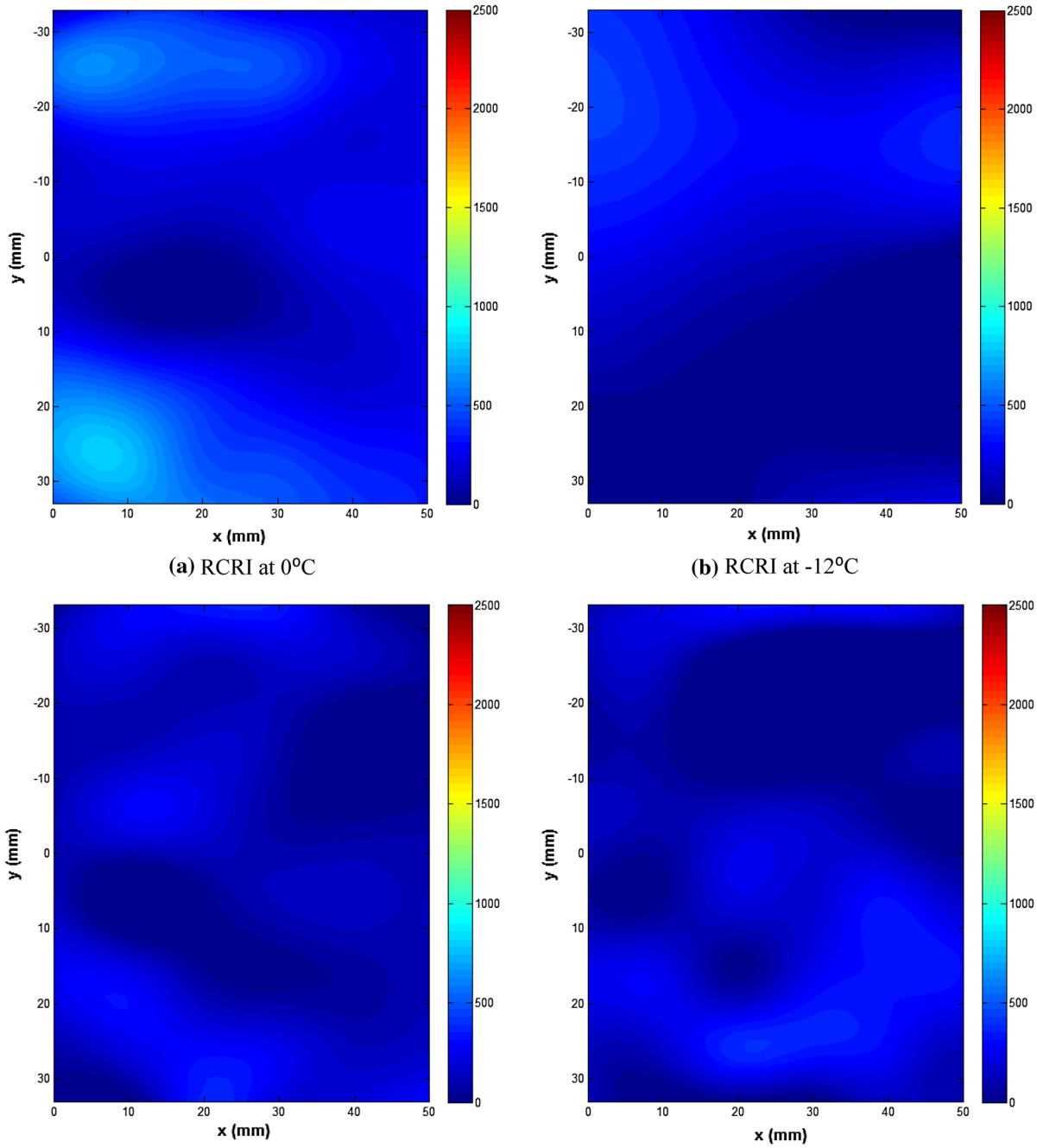

(a) RCRI at 0°C

(b) RCRI at -12°C

(c) PG 64-22 at -0°C

(d) PG 64-22 at -12°C

Fig. 6 DIC ε_{yy} Fields at 2.0 kN (με)

concrete. A Double Shear Test (DST) was used to determine the shear crack propagation rate at the interface of two layers. The advantage of the DST over single interlayer shear test methods is that the two interfaces symmetrically undergo a relatively pure shear stress, whereas the single interlayer tests have problems with bending and normal forces at the interface and in areas close to the two ends of specimen [9].

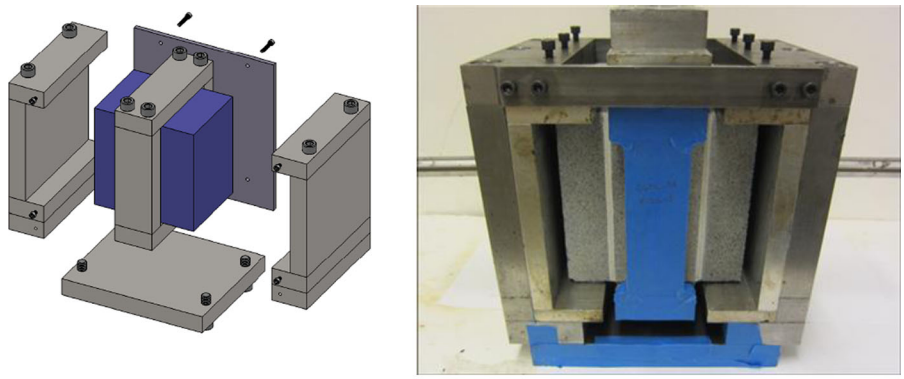

(a) original DST design **(b)** final version of DST device

Fig. 7 DST before and after changes

4.1 Materials and experimental methodology

In this study a mix obtained from Rea Contracting Company in Raleigh, North Carolina, (RS9.5B) was used in making hot mix asphalt (HMA) grid-reinforced slabs.

In the double shear test, the side parts of the sample are fixed and the middle is subjected to loading. A specific DST device was designed and fabricated based on the optimum required size of the specimen and the grid opening size. The dimensions of the interface were chosen to be 15.24 cm in the direction of compaction by 11.43 cm in the transverse direction in order to have an acceptable shear stress distribution and also a good number of ribs within each specimen.

The original design of the DST device consists of three parts: two parts on either side and one belt-like part in the middle (Fig. 7a). Each part is glued to the specimen. The middle part is free to move up and down, and the sides are fixed to the base plate. Figure 7b shows the device after making some changes to the original design to make the device capable of running multiple consecutive tests without changing the main parts.

For a better understanding of the interface shear performance of specimens reinforced with grid, DSTs were performed on specimens that were made from HMA slabs. The testing temperature was 20 °C, and the number of replicates for each condition was three. All the specimens were kept in the testing climate chamber for three hours at 20 °C before testing. The tests were carried out in load control mode. A sinusoidal alternating load with a frequency of 5 Hz and a zero mean was applied to the middle part of the shear specimens using an MTS 810 servo-hydraulic material testing system. Digital image correlation (DIC) was used to track and measure the deformations, displacements, and strains on the surface of the specimens and especially in the areas around the interlayer. A 5 MP camera along with a National Instruments high-speed multifunction DAQ were used. The specimens were speckled in a random pattern with a white background and black dots to allow for image analysis (Fig. 8). The camera was placed 80 cm from the surface of each sample to capture the images. VIC-2D (Correlated Solutions [6]) software was used to analyze the images. A subset size of 23 × 23 was chosen for the analysis, which covers a 2-mm square on the surface of the specimens.

Fig. 8 Speckled surface of a shear specimen

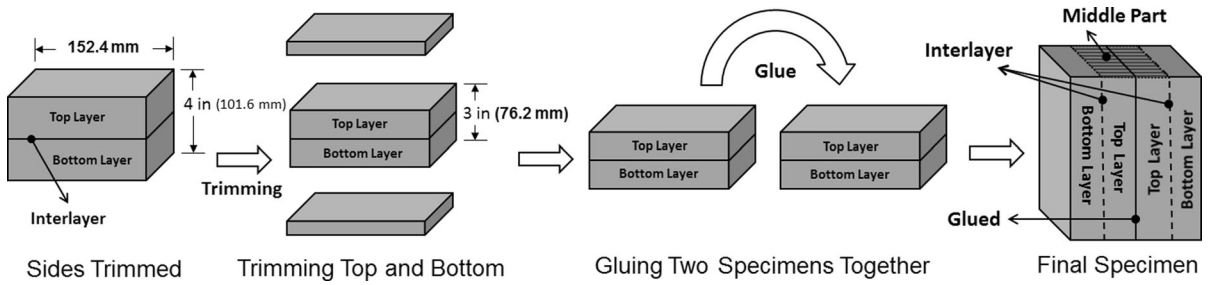

Fig. 9 DST specimen preparation procedure

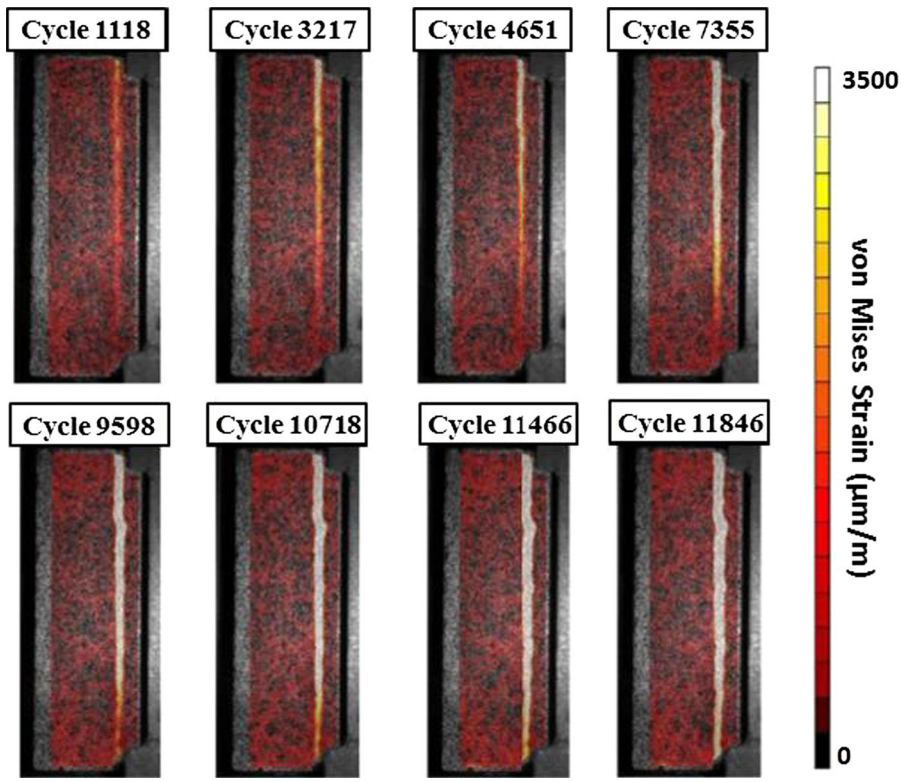

Fig. 10 Von Mises strain contour evolution at different numbers of cycles (the first approach)

4.2 Specimen preparation

The DST specimens consist of three layers bonded together with the same interlayer characteristics. Two sides are fixed, and the central layer, which is subjected to loading, is free to move. The specimens were made by cutting two rectangles out of slabs, trimming them and gluing the top surfaces together. Each rectangular part is 15.24 cm long, 11.43 cm wide, and 7.62 cm thick after trimming. Figure 9 presents the specimen preparation procedure. By following this method of sample preparation, both interfaces have the same characteristics in terms of compaction, roughness, interlayer systems, tack coat application rate, and age.

4.3 Test results and discussion

The main challenge in the analysis of the DST data was determining the length of the cracks during the tests. Three different approaches were used to find the crack tip: strain contour, visual detection, and a bisectional approach.

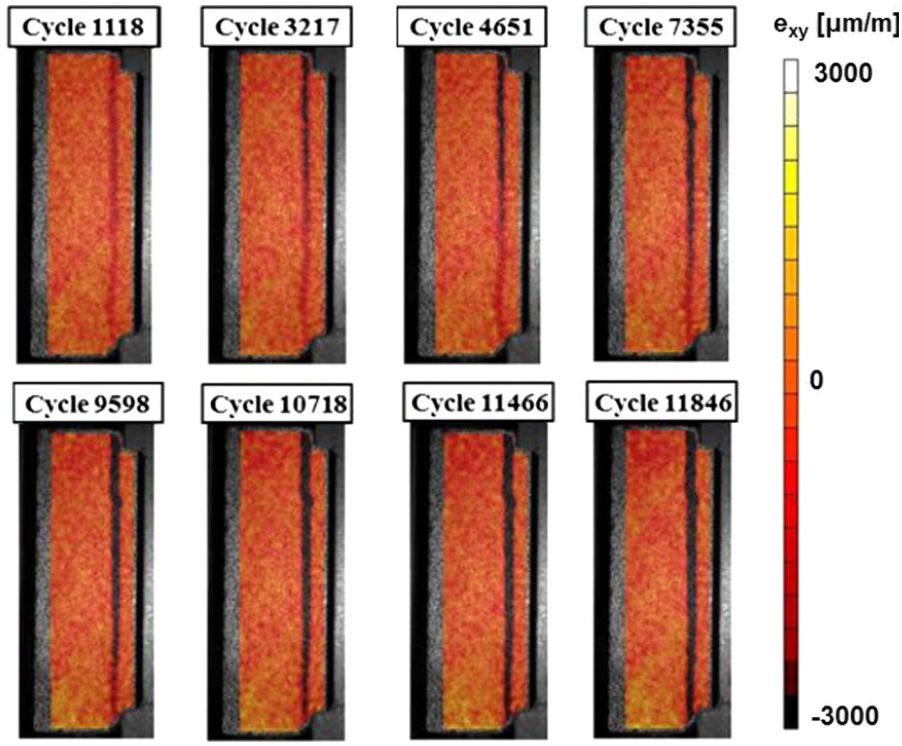

Fig. 11 Shear strain contour evolution at different numbers of cycles (the first approach)

4.3.1 Strain contour

By utilizing DIC, the displacements and strains of the surface of a specimen can be tracked. Figures 10 and 11 present the evolution of the Von Mises and shear strain contours of the specimen, respectively. These figures show a continuous increase in strain amplitude throughout the testing. This increase is more obvious around the interlayer and represents the crack propagation and failure process of the specimen. Two main problems are inherent of this strain contour approach. The first problem is the error or noise of the strain results that is sometimes as high as 300 μstrain without applying any load, or even higher when the specimen starts to deform and crack. The second problem is determining the strain threshold of cracking or failure for the different conditions. It is difficult to find a certain number or range of numbers for the strain at which the crack appears.

4.3.2 Visual detection

The second approach was investigated using a speckled sample that was painted white along both interlayers. The purpose of this approach is to correlate the displacement or relative displacement results with the crack propagation. This approach failed because the shear crack is extremely fine around the crack tip and difficult to detect, especially with the current camera setup in the lab. Another problem is that, because the paint and the interface condition were not compatible, a crack in the paint is not necessarily a good representation of the interface crack.

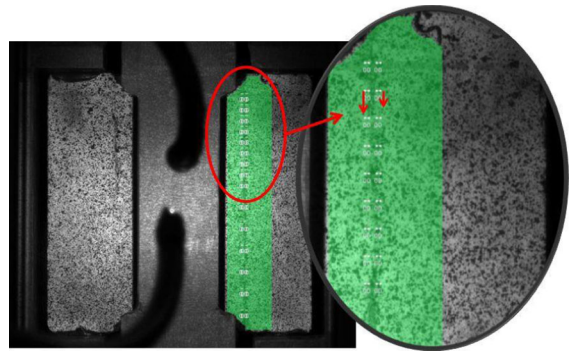

Fig. 12 Virtual gauges defined at certain positions (the third approach)

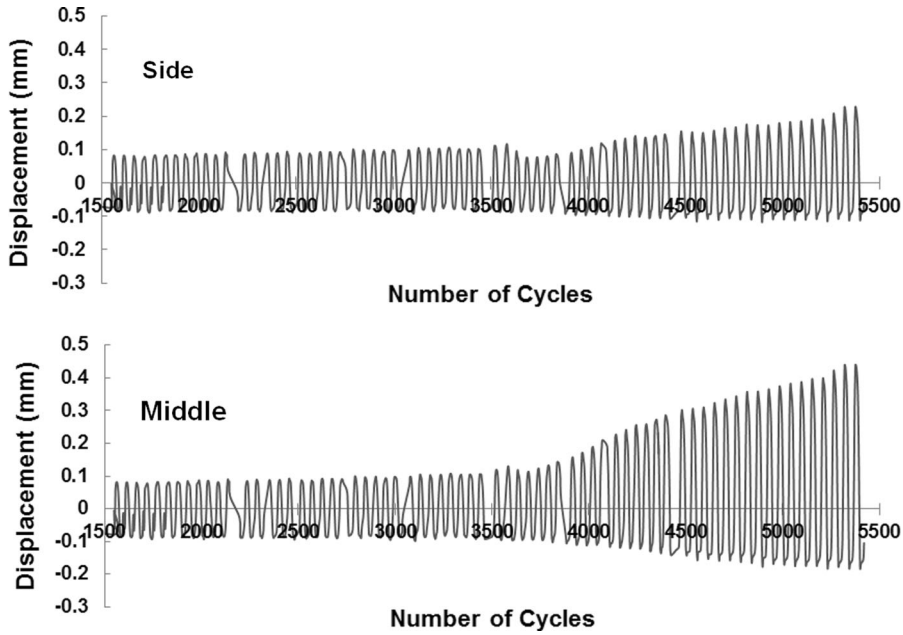

Fig. 13 Displacement of the gauges located in the middle part and side part of the specimen

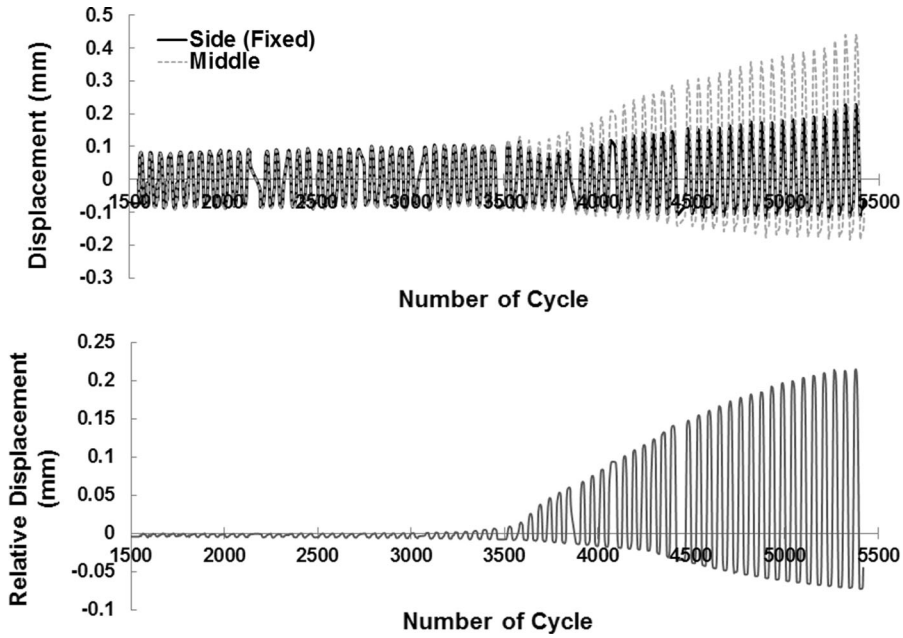

Fig. 14 Bisectional approach for finding the crack length

4.3.3 Bisectional approach

The third approach is a bisectional approach. As shown in Fig. 12, sets of virtual gauges were used at certain positions to track the displacements on opposite sides of the interlayer throughout the test.

Figure 13 shows an example of the displacement of two gauges at the same level and located at the sides of the interface. The gauges were 2 mm away from the interface and have a length of 1 mm. Each of these virtual gauges consists of 101 points, and the displacement reported by each gauge is the average displacement of these points. An estimate of the shear occurring along the interface can be obtained by calculating the relative displacements of the virtual gauges on opposite sides of the interface. From plots of

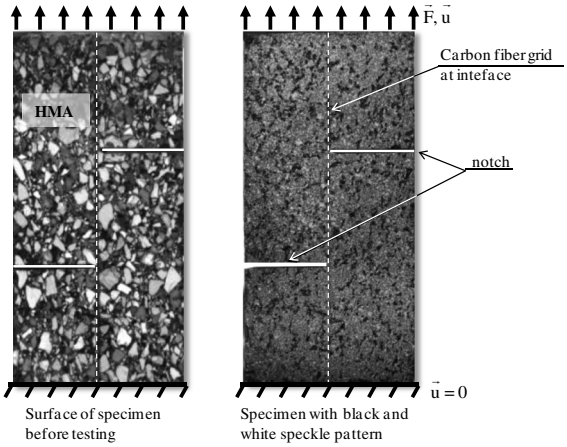

Fig. 15 Double notch shear test (specimen geometry with loading configuration)

the relative displacement versus number of cycles it can be observed that the relative displacement increases almost linearly with the increase of the number of load cycles until a point at which the two gauges seem to start moving more independently. This point is correlated with the crack growth and failure of the interface between the two gauges. Figure 14 shows that, even though after this point the curve starts to deviate from the virtual linear line, there is still some shear resistance that is related to aggregate interlock at the interface. Romanoschi and Metcalf [20] reported the same interface behavior under shear fatigue testing.

It is assumed that this deviation point is the failure point. By looking at the relative displacements versus number of cycles at different positions, the crack propagation and growth rate can be determined. This information can be used to find fracture-related properties of the specimen.

5 Application of DIC techniques on debonding

This section explores application of DIC to investigate shear-banding and debonding effects in bi-layered asphalt concrete reinforced with carbon fiber grid. The carbon fiber grid may increase stiffness of the pavement. Consequently, it is important to understand the material failure along interface. A double notch shear specimen was used to observe shear band thickness at the interface. The testing configuration.

This test series aimed at providing some insight the interface behavior with damage evolution and scale effect (depending on size of aggregate).

5.1 Materials and methods

A picture of the test setup and the specimen geometry can be seen in Fig. 15. This double notch shear specimen consists of bi-layered HMA with Carbon Fiber grid at the interface. The tested material was provided in the RILEM-SIB in TG4 (Réunion Internationale des Laboratoires et Experts des Matériaux - Testing and characterization of Sustainable Innovative Bituminous materials and systems, Task Group 4: Pavement Multilayer System Testing). The test configuration and the specimen geometry induce a pure shear loading at the interface. As regard the test boundary conditions, the bottom of specimen is fixed on the testing machine by rigid connections, when the top end is loaded in tension. The test are performed under displacement control with the cross bar rate of 0.5 mm/sec.

During loading the force/displacement evolution is measured by means of LVDT position sensor and a load cell of 50kN.

The deformations on the specimen surface are measured by means of DIC method. These measurements allowed for determining displacement and strain fields, and investigate debonding behavior at the interface. The DIC configuration used consisted of an AVT Marlin F-201B with a Pentax 12.5-75 mm lens and a LED light source. The monochrome CCD camera resolution is 1,628(H) × 1,236(V) pixels which captured image at a rate of 15 images/s at full resolution. Correla software, developed by PEM team of Pprim Institute of Poitiers, is used to perform DIC. The estimating uncertainty of displacement is 0.026 pixels.

As is shown in Fig. 15, prior to testing, a black and white speckle pattern is sprayed on the specimen surface. This random distribution of gray follows material deformation.

5.2 Test results

The force/displacement relationships are presented in Fig. 16. LVDT are used to measure the top displacement of specimen. In the graph it can be seen that specimen failure is not a brittle failure mainly due to the carbon fiber grid at the interface. From the force/displacement relationships the evolutions of energies were

determined. The total strain energy is equal to the area under the force/displacement curve. The elastic strain energy is assimilated with the energy that may be recovered when loading is gradually removed. In the graph of energy evolution it can be seen a significant amount of dissipated energy in the damage and debonding process. This aspect will be highlighted in DIC analysis.

In a first view, a maximum loading for 1 mm of displacement can be observed. At this load step no significant observations on energy, except a relative low dissipated energy just before the peak. So the main

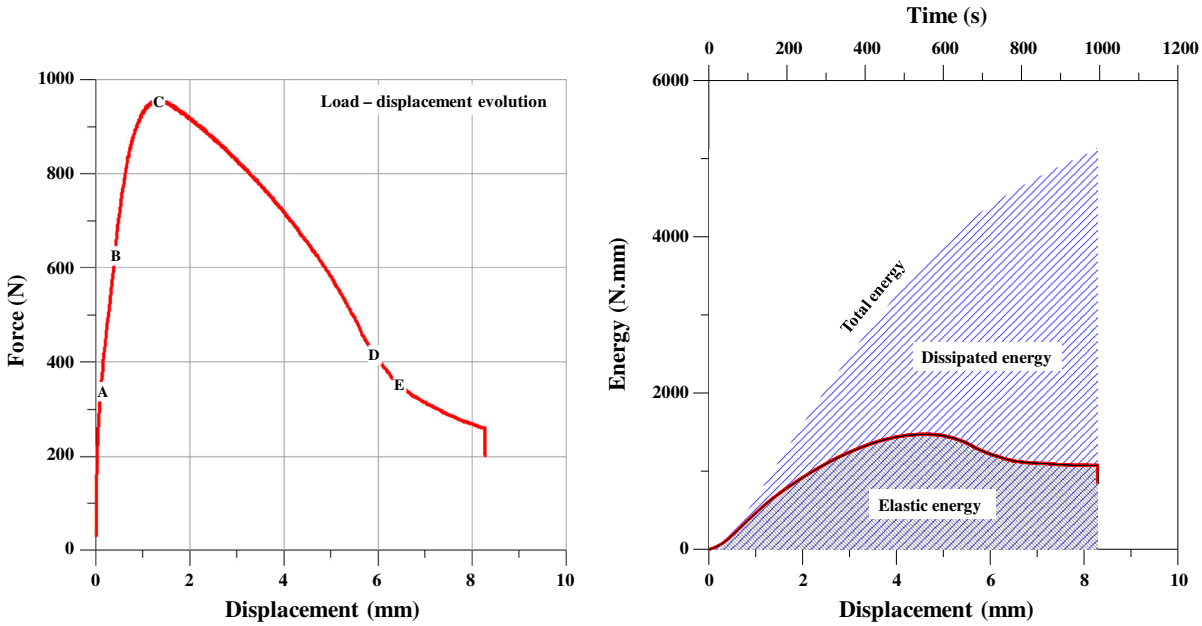

Fig. 16 Force/displacement and energy evolution curves

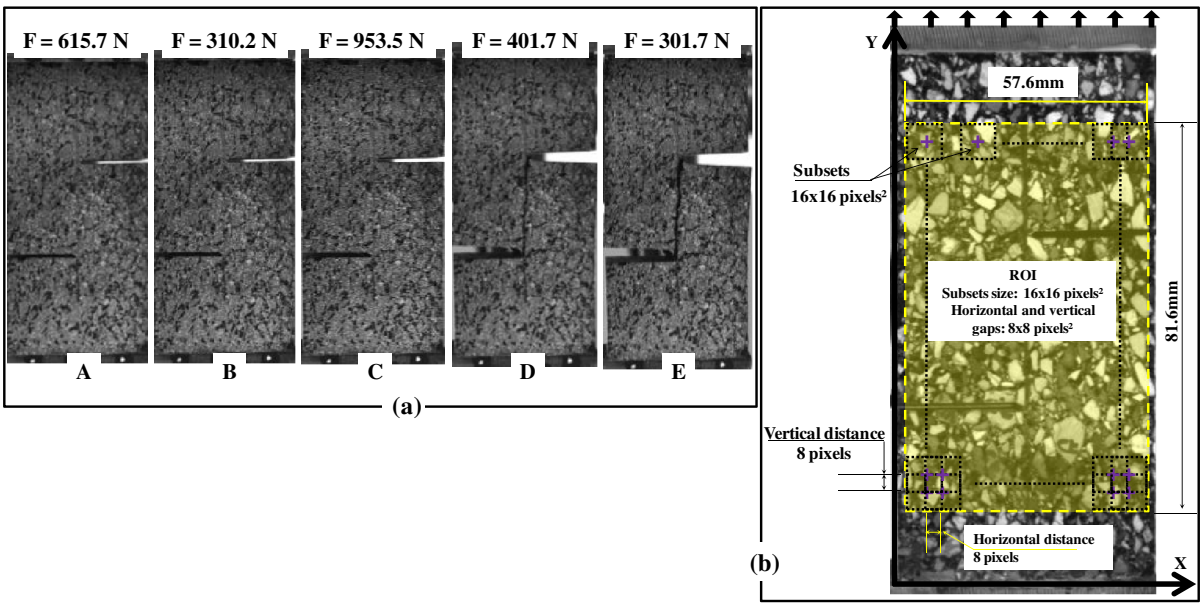

Fig. 17 Images of observed damage and DIC analysis

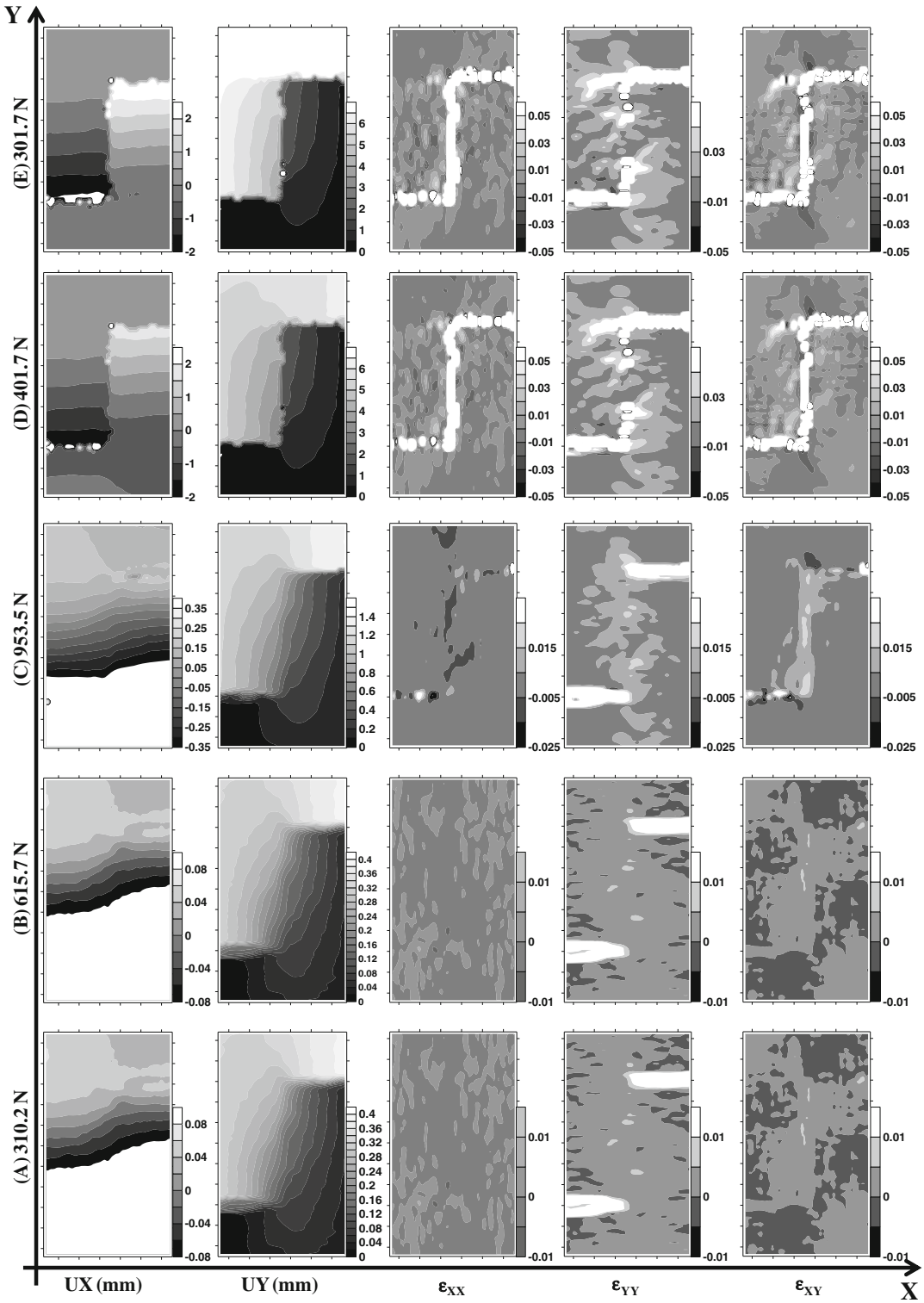

Fig. 18 Displacement and strain fields inside ROI

dissipated energy is observed after the peak during softening, probably consumed in the interface and CF grid deformation.

Figure 17(a) shows the images of observed damage for the five load steps shown in Fig. 16. Analysis reveals that the debonding at interface begins once the maximum loading is exceeded.

The displacement and strain field's evolutions were measured using the optical measurement and calculated along a Region Of Interest (ROI) of size 57.6 by 81.6 mm. The ROI discretized using subsets size of 16 by 16 pixels is shown in Fig. 17b. The horizontal and vertical distance between two subsets is 8 by 8 pixels. It should be noted that the scale factor is 0.15pixels/mm. The frame rate of camera 1images/sec.

The DIC results in terms of displacement and strain fields in the horizontal (X) and the vertical (Y) directions are provided in Fig. 18. The displacements are defined by a plane material transformation composed of 2 rigid displacement parameters (UX, UV) and 4 local gradients parameters ($\partial UX/\partial x$, $\partial UX/\partial y$, ($\partial UY/\partial x$, $\partial UY/\partial y$). The components of the gradient are calculated by finite differences. As previously the mechanical fields are computed for the five load steps shown in Fig. 16.

The analysis of displacement and strain fields from mechanical tests, lead us to conclude that:

- UX is very interesting to show that the shear loading induce normal displacement (dilatancy) and debonding can be observed after 4th image. The UX fields enable us to identify debonding normal to the interface.
- UY can be used to identify the shear band thickness which can be assumed as an internal length. This thickness is constant during loading except close to failure when the localization appears thickness go to zero (4th and 5th image).
- ε_{xx} is very interesting to comment because the shear loading is not pure and induces normal tensile strains and stresses which lead to the interface debonding. It seems that localized tensile strain begin close to the notches in the interface surface.
- ε_{yy} is practically not concerned in the debonding behavior, only the opening notches can be shown.
- ε_{xy} is the main shear loading and the localization is observed in the beginning of loading (1st image). ε_{xy} fields show that the shear occurring at interface.

ε_{xy} and UX analysis enables a kinematics localization of shear-banding and debonding along interface. Even though we do not describe the micromechanical behavior inside the shear bands, the data obtained from the optical measurements by DIC reveal that band dimensions are the aggregate size scale.

Contrarily to visual observations, the DIC shows that the degradation of interface emerges before the peak loading, and becomes more expansive with post-peak softening. The displacement and strain cartographies reveal that the formation of shear banding occurs prior to damage and the damage is a consequence of shear band formation.

The correlation between the force/displacement curve and the mechanical fields show that when the softening grows the localization zones widen while centered in the pure shear direction with its edges remaining parallel.

The data obtained from the optical measurements by DIC show that the debonding process results from a combination between mode I and II. It is due to real experimental boundary conditions and the sample geometry.

All the above observations, lead us to conclude that the following sequence of events must be incorporated modeling of deformation and debonding of bi-layered HMA with carbon fiber grid at the interface:

- Strain localization occurs at small deformation due to heterogeneous nature of material;
- Shear bands arise from geometric dimensions of aggregate;
- Debonding and final failure appear in the shear band localized along interface.

6 Summary and conclusions

Digital image correlation (DIC) appears the most suited image processing technique for asphalt mixture investigation since it has shown to adequately detect anisotropies and heterogeneities typical of bituminous materials, i.e. defect or cracks within the skeleton. DIC has proven to overcome the limitations of traditional displacement/strain measurement techniques (e.g. strain gauges and LVDTs), achieving satisfactory accuracies. It has been shown that DIC techniques are adequate for investigating very important cracking phenomena in asphalt mixtures as Mode I and Mode II crack propagation and debonding.

The most important advantages of using DIC for asphalt mixture testing can be summarized as follows:

- It is a noncontact technique; this reduces setup timing and mounting errors;
- it provides pointwise analysis pinpointing the location of crack initiation;
- it accounts for non-uniform strain distributions (i.e. fracture process zone);
- it provides flexibility since it allows a "back analysis" of the resulting strain field over an area of finite extent, preventing to mount multiple sensors in different locations.

References

1. Birgisson B, Montepara A, Romeo E, Roque R, Roncella R, Tebaldi G (2007) Determination of fundamental tensile failure limits of mixtures. J Assoc Asph Paving Technol 76:303–344
2. Birgisson B, Montepara A, Romeo E, Roque R, Roncella R, Tebaldi G (2009) An optical strain measurement system for asphalt mixtures. Mater Struct 42(4):427–441. doi:10.1617/s11527-008-9392-8
3. Birgisson B, Montepara A, Romeo E, Roque R, Tebaldi G (2010) Influence of mixture properties on fracture mechanics in asphalt mixtures. Road Mater Pavement Des 11:68–88. doi:10.3166/rmpd.11hs.61-88
4. Chehab GR, Kim YR, Schapery R, Witzack M, Bonaquist R (2003) Characterization of asphalt concrete in tension using a viscoelastoplastic model. J Assoc Asph Paving Technol 72:315–355
5. Chehab GR, Seo Y, Kim YR (2007) Viscoelastoplastic Damage Characterization of Asphalt-Aggregate Mixtures using Digital Image Correlation. Int J Geomech 7(2):111–118. doi:10.1061/(ASCE)1532-3641(2007)7:2(111)
6. Correlated Solutions http://www.correlatedsolutions.com/vic-2d/. Accessed 25 July 2013
7. Dave EV, Braham AF et al (2008) Integration of laboratory testing, field performance data and numerical simulations for the study of low-temperature cracking. In: Al-Qadi L, Scarpas T, Loizos A (eds) Proceedings of the 6th RILEM International Conference on Cracking in Pavements, Chicago. CRC Press; Taylor and Francis Group, New York, pp 369–378
8. Dave EV, Ahmed S, Buttlar WG, Bausano JP, Lynn T (2010) Investigation of strain tolerant mixture reflective crack relief systems: an integrated approach. J Assoc Asphalt Paving Technol 79:119–156
9. Diakhate M, Phelipot A, Millien A, Petit C (2006) Shear fatigue behaviour of tack coats in pavement. J Road Mater Pavement Des 7(2):201–222
10. Hartman AM, Gilchrist MD (2004) Evaluating four-point bend fatigue of asphalt mix using image analysis. J Mater Civ Eng 16(1):60–68. doi:10.1061/(ASCE)0899-1561(2004)16:1(60)
11. Im S, Kim YR, Ban H (2013) Rate- and temperature-dependent fracture characteristics of asphaltic paving mixtures. ASTM J Test Eval 41(2):1–12. doi:10.1520/JTE20120174
12. Kim YR, Little DN (1990) One-dimensional constitutive modeling of asphalt concrete. J Eng Mech 116(4):751–772. doi:10.1061/(ASCE)0733-9399(1990)116:4(751))
13. Kim YR, Wen H (2002) Fracture Energy from Indirect Tension Test. J Assoc Asph Paving Technol 71:779–793
14. Lecompte D, Smits A, Bossuyt S, Sol H, Vantomme J, Van Hemelkijck D, Habraken AM (2006) Quality assessment of speckle patterns for digital image correlation. Opt Lasers Eng 44(11):1132–1145. doi:10.1016/j.optlaseng.2005.10.004
15. Marasteanu M et al (2012) Investigation of low temperature cracking in asphalt pavements national pooled fund study—phase II, Report No. MN/RC 2012-23, Minnesota Department of Transportation, St. Paul, MN
16. Masad E, Muhunthan B, Shashidhar N, Harman T (1998) Aggregate orientation and segregation in asphalt concrete. In: Proceedings of sessions of geo-congress on application of geotechnical principles in pavement engineering, pp 69–80
17. Masad E, Muhunthan B, Shashidhar N, Harman T (1999) Internal structure characterization of asphalt concrete using image analysis. J Comput Civ Eng 13(2):88–95. doi:10.1061/(ASCE)0887-3801(1999)13:2(88)
18. Masad E, Somadevan N, Bahia HU, Kose S (2001) Modeling and experimental measurements of strain distribution in asphalt mixes. J Transp Eng 127(6):477–485. doi:10.1061/(ASCE)0733-947X(2001)127:6(477)
19. Montepara A, Romeo E, Birgisson B, Tebaldi G (2010) Strain localization and damage distribution in SBS polymer modified asphalt mixtures. Road Mater Pavement Des 11(4):899–915. doi:10.3166/rmpd.11.899-915
20. Romanoschi SA, Metcalf JB (2001) The characterization of asphalt concrete layer interfaces. 80th Annual TRB Meeting. Transportation Research Board, Washington, DC
21. Romeo E (2013) Two-dimensional digital image correlation for asphalt mixture characterisation: interest and limitations. Road Mater Pavement Des. doi:10.1080/14680629.2013.815128
22. Roque R, Birgisson B, Sangpetgnam B, Zhang Z (2002) Hot mix asphalt fracture mechanics: a fundamental crack growth law for asphalt mixtures. J Assoc Asph Paving Technol 71:816–827
23. Schreier HW (2003) Investigation of two and three-dimensional image correlation techniques with applications in experimental mechanics. PhD Thesis, University of South Carolina, Columbia, SC
24. Seo Y, Kim YR, Schapery R, Witczac M, Bonaquist R (2004) A study of crack-tip deformation and crack growth in asphalt concrete using fracture mechanics. J Assoc Asph Paving Technol 73:697–730
25. Shen B, Paulino GH (2011) Direct extra direct extraction of cohesive fracture properties from digital image correlation: a hybrid inverse technique. J Exp Mech 51:143–163. doi:10.1007/s11340-010-9342-6
26. Sutton MA, McNeill SR, Helm JD, Chao YJ (2000) Advances in two-dimensional and three-dimensional computer vision photomechanics. Top Appl Phys 77:323–372. doi:10.1007/3-540-48800-6_10
27. Sutton MA, Li N, Joy DC, Reynolds AP, Li X (2007) Scanning electron microscopy for quantitative small and

large deformation measurements: part I. SEM imaging at magnifications from 200 to 10,000. Exp Mech 47(6):775–787. doi:10.1007/s11340-007-9042-z
28. Sutton MA, Yan JH, Tiwari V, Schreier WH, Orteu JJ (2008) The effect of out-of-plane motion on 2D and 3D digital image correlation measurements. Opt Lasers Eng 46(10):746–757. doi:10.1016/j.optlaseng.2008.05.005
29. Tashman L, Wang L, Thyagarajana S (2007) Microstructure characterization for modeling HMA behaviour using imaging technology. Road Mater Pavement Des 8(2):207–238. doi:10.1080/14680629.2007.9690073
30. Thiago AF, Kim YR (2011) Characterization of fracture properties of asphalt mixtures based on cohesive zone modeling and digital image correlation technique. In: 90th Annual meeting of the transportation research board, Washington
31. Wagoner MP, Buttlar WG, Paulino GH, Blankenship P (2005) Investigation of the fracture resistance of hot-mix asphalt concrete using a disk-shaped compact tension test. Transp Res Rec 1929:183–192
32. Zhang Z, Roque R, Birgisson B, Sangpetgnam B (2001) Identification and verification of a suitable crack growth law. J Assoc Asph Paving Technol 70:206–241